Postseismic backslip as a response to a sequential elastic rebound of upper plate and slab in subduction zones

Ehsan Kosari[1,2], Matthias Rosenau[1], Thomas Ziegenhagen[1], and Onno Oncken[1,2]

[1] Helmholtz Centre Potsdam, GFZ German Research Centre for Geosciences, Potsdam, Germany.

[2] Department of Earth Sciences, Freie Universität Berlin, Berlin, Germany.

Corresponding author: Ehsan Kosari (ehsan.kosari@gfz-potsdam.de)

Key Points:

- Analog megathrust earthquake experiments provide high-resolution observations to evaluate the elastic-frictional signal from the shallow megathrust
- Surface displacement time-series suggest a sequential elastic rebound of the upper plate and slab
- A combination of the slab's rebound and the rapid relaxation of the upper plate may accelerate the backslip

Abstract

An earthquake-induced stress drop on a megathrust instigates different responses on the upper plate and slab. We mimic homogenous and heterogeneous megathrust interfaces at the laboratory scale to monitor the strain relaxation on the two elastically non-identical plates by establishing analog velocity weakening and strengthening materials. A sequential elastic rebound follows the coseismic shear-stress drop in our elastic-frictional models: a fast rebound of the upper plate and the delayed and smaller rebound on the slab. A combination of the delayed rebound of the slab and the rapid relaxation of the upper plate after an elastic overshooting may accelerate the relocking of the megathrust. This acceleration triggers/antedates the failure of a nearby asperity and enhances the early backslip in the rupture area. Consequently, the trench-normal rearward displacement in the upper plate may reach a significant amount of the entire interseismic backslip and speeds up the stress build-up on upper plate faults.

Plain Language Summary

Subduction zones, where one tectonic plate slides underneath the other, host the largest earthquakes on earth. Two plates with different physical properties define the upper and lower plates in the subduction zones. A frictional interaction at the interface between these plates prevents them from sliding and builds up elastic strain energy until the stress exceeds their strength and releases accumulated energy as an earthquake. The source of the earthquake is located offshore; hence illuminating the plates' reactions to the earthquakes is not as straightforward as the earthquakes occur inland. Here we mimic the subduction zone at the scale of an analog model in the laboratory to generate analog earthquakes and carefully monitor our simplified model by employing a high-resolution monitoring technique. We evaluate the models to examine the feedback relationship between upper and lower plates during and shortly after the earthquakes. We demonstrate that the plates respond differently and sequentially to the elastic strain release: a seaward-rearward motion of the upper plate and an acceleration in the lower plate sliding underneath the upper plate. Our results suggest that these responses may trigger another earthquake in the nearby region and speed up the stress build-up on other faults.

1 Introduction

A massive megathrust earthquake (Mw≥8) causes a shear stress drop on the subduction interface that drives the subduction system from a quasi-steady state in the interseismic loading stage to a temporarily unstable relaxation mode. This postseismic destabilization triggers different reactions over the shallow and deep parts of the subduction system, which are rheologically dominated by elastoplastic and viscoelastic behavior, respectively (e.g., Wang *et al*., 2012; Weiss *et al.*, 2019). To date, we identified several postseismic processes that can be seismic and aseismic, namely (1.) afterslip along the megathrust (e.g., Hsu *et al.*, 2006; Bedford *et al.*, 2013; Hoffmann *et al.*, 2018), (2.) viscoelastic relaxation of the lower crust and mantle of both slab and upper plate (e.g., S. Li et al., 2015; Sun et al., 2014) and (3.) crustal faulting in the upper plate (extensional), accretionary wedge (compressional), and shallow slab (extensional) (e.g., Kato et al., 2011; Hicks and Rietbrock., 2015; Hoskins *et al.*, 2021).

A coupled elastic-viscous response of the subduction system to a megathrust stress-drop by multiple mechanisms makes the postseismic signals more convoluted. Only a handful of megathrust earthquakes are relatively densely monitored. In many of these cases, the postseismic surface displacement above the ruptured asperity exhibits intriguing signals from depth that are interpreted differently (e.g., Bedford et al., 2016; Heki & Mitsui, 2013; Tomita et al., 2017; Watanabe et al., 2014). While the postseismic viscoelastic signal from the relaxing asthenosphere appears with a characteristic long-term pattern and large-scale wavelength (far-field, hundreds of kilometers scale) (e.g., Wang *et al.*, 2012; Sun and Wang, 2015), the postseismic elastic-frictional processes (i.e., relocking and afterslip) show relatively steep gradients and short-wavelength (tens of kilometers scale) characteristics. These short-wavelength postseismic signals interfere in the near-field with the presumably more steady interseismic re-loading process that has a reverse kinematic sense (i.e., landward motion in the upper plate). Such interference perturbs a relatively smooth and homogeneous surface displacement above the ruptured patched and nearby regions manifested by short time and short distance changes in amplitude and direction causing shear and vertical axis rotations. Such "enigmatic patterns" are notoriously difficult to interpret, and discourse is rising about its relevance for seismic hazard (e.g., Loveless, 2017; Melnick *et al.*, 2017; Yuzariyadi and Heki, 2021). We here contribute to this discussion using observations and interpretations of controlled experiments highlighting the potential variability of deformation signals in subduction zones.

The elastic-frictional displacement signals from the shallow part of the megathrust are often poorly documented. The upper plate and slab experience non-identical elastic rebounds. Moreover, the stress state (pre- versus post-event) close to the interface presents more complex slip behavior (i.e., opposite senses of shear in a short time) than a simple shear-stress drop (e.g., Brodsky *et al.*, 2020). Hence, it remains unclear how the elastic interrelationship between the upper- and lower plates may contribute to this domain's surface signals. This study aims to address the sequential upper plate and slab elastic-frictional response during the nearly complete coseismic shear-stress drop and its early postseismic stage in a subduction megathrust system by employing a series of carefully monitored analog modeling experiments. To examine the feedback relationship between the upper plate and the slab, we investigate two generic seismotectonic scale models representing homogeneous and heterogenous subduction megathrust systems and capture the model's surface displacements by employing a high resolution and high speed "laboratory geodetic" method.

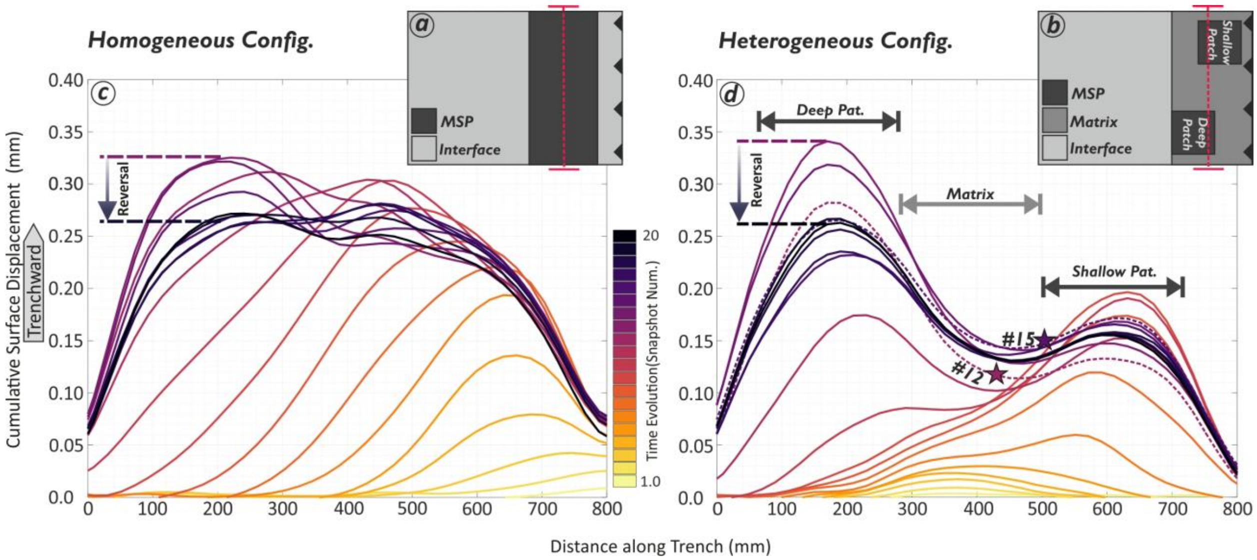

Figure 1. Model setup and exemplary evolution of coseismic and early-postseismic surface deformation in two scenarios. a and b: Plan view of the seismotectonic scale models' configurations (Figure S1); Light, medium, and dark gray colors represent the velocity strengthening ("aseismically" creeping) interface, a velocity weakening matrix characterized by microslips ("microseismicity"), and the main slip patch(es) (MSP) where large analog megathrust earthquake slip occurs ("seismogenic zone" or "asperity"), respectively. The red dashed lines show the profiles along which the cumulative surface displacement is shown in c and d. The downward vectors indicate surface displacement reversal during the early-postseismic stage interpreted as backslip. The stars on the dashed lines show the selected snapshots for slip modeling in Figure 2.

2 Methodology

2.1 Seismotectonic scale modeling

Seismotectonic scale models have been established to generate physically self-consistent analog megathrust earthquake ruptures and seismic cycles at the laboratory scale (Rosenau et al., 2009; 2017, and references therein). They have been used to study the interplay between short-term elastic (seismic) and long-term permanent deformation (Rosenau & Oncken, 2009), earthquake recurrence behavior and predictability (Corbi et al., 2020; 2019; 2017; Rosenau et al., 2017), the linkage between offshore geodetic coverage and coseismic slip model (Kosari et al., 2020) and details of the seismic cycle (Caniven & Dominguez, 2021). Analog models are downscaled from nature for the dimensions of mass, length, and time to maintain geometric, kinematic, and dynamic similarity by applying a set of dimensionless numbers (King Hubbert, 1937; Rosenau et al., 2009; 2017). The models generate a sequence of tens to hundreds of analog megathrust earthquake cycles, allowing the analysis of the corresponding surface displacement from dynamic coseismic to quasi-static interseismic stages.

In the presented 3-D experimental setup modified from Rosenau *et al.* (2019) and introduced in Kosari *et al.* (2020), a subduction forearc model is set up in a glass-sided box (1,000 mm across strike, 800 mm along strike, and 300 mm deep) with a 15° dipping, elastic basal rubber conveyor belt (the model slab), and a rigid backwall. A flat-topped wedge made of an elastoplastic sand-rubber mixture (50 vol.% quartz sand G12: 50 vol.% EPDM-rubber) is sieved into the setup representing a 240 km long forearc segment from the trench to the volcanic arc (Figures 1a and b; and S1).

At the base of the wedge, zones of velocity weakening controlled stick-slip (“seismic” behavior) are realized by emplacing compartments of either flavored rice (“main slip patches”) or fine table salt (“matrix”), which generate quasi-periodic large and small slip instabilities, respectively (Figures 1a, b, and S1), mimicking megathrust earthquakes of different size and frequency. Large stick-slip instabilities in the main slip patch(es) (MSP) are almost complete and recur at low frequency (~0.2 Hz), while those in the matrix are partial (<10%) and at high frequency (~10 Hz) at a prescribed constant convergence rate of 50 µm/s. This bimodal behavior is intended to mimic rare great (M8-9) earthquakes versus small frequent repeating events (e.g., Uchida and Bürgmann, 2019; Chaves *et al*., 2020) in a creeping environment akin to concepts of the shallow subduction megathrust (e.g., Bilek and Lay, 2002). The wedge itself and the conveyer belt respond elastically to these basal slip events similar to crustal rebound during natural subduction megathrust earthquakes. Upper plate faults (in our case, a single backthrust fault) gradually emerge downdip and up-dip of the main slip patches over multiple seismic cycles, as documented in earlier papers (Kosari et al., 2020; Rosenau et al., 2009, 2010; Rosenau & Oncken, 2009).

Two different configurations of analog earthquake behavior have been considered for the shallow part of the wedge base representing the seismogenic zone of the subduction plate interface. In the first configuration, hereafter named “homogeneous configuration”, a single large rectangular stick-slip patch (Width*Length=200*800 mm) is implemented as the main slip patch (MSP), representing a system of a homogeneous seismogenic zone with temperature-controlled depth range and no variation along strike generating M9 type megathrust events similar to the 2014 Sumatra earthquake. In the second case, hereafter named “heterogeneous configuration”, two square-shaped MSPs (200*200mm) have been emplaced, acting as two medium-size seismogenic asperities generating M8-9 type events similar to the 2010 Maule earthquake. These patches are at a center-to-center distance of 400mm and 100mm in trench-parallel and trench-normal direction, respectively, while they are surrounded by a matrix hosting frequent small events (Figures 1 and S1).

2.2 Laboratory geodesy

To capture horizontal micrometer-scale surface displacements associated with analog earthquakes at microsecond scale periods, we monitor the model surface with a highspeed CMOS (Complementary Metal Oxide Semiconductor) camera (Phantom VEO 640L camera, 12 bit, 4 MPx) intermittently at 250 Hz (Figure S1). Digital image correlation (e.g., Adam et al., 2005) has been applied via the DAVIS 10 software (LaVision GmbH, Göttingen/DE). Data are processed to yield observational data similar to those from an ideal dense and full coverage (on- and offshore) geodetic network, that is, velocities (or incremental displacements) at locations on the model surface. We use an analog geodetic slip inversion technique (AGSIT, Kosari et al,. 2020) to invert surface displacements for model megathrust slip and backslip distribution over earthquake cycles. Note that although all observations can be upscaled to nature using scaling laws (King Hubbert, 1937; Rosenau et al., 2017, 2009), we report here all values at the laboratory scale.

3 Results: Observations and interpretations

In the following, we analyze a high-resolution time-series of surface and slab displacements and slip along the megathrust and an emergent upper plate fault over several seismic cycles. We analyze both the heterogeneous (which is at the center of focus here) and homogeneous configurations to capture the details of upper plate and slab responses in the coseismic and early-postseismic stages (Figures 1c, d, and 3). We discuss the Coulomb Failure Stress Change (ΔCFS) over coseismic and early-postseismic stages and its impact on model slab velocity changes (Figures 2,3). Subsequently, we evaluate the elastic rebound of the slab and the upper plate in response to the mainshock-induced stress changes. Finally, we explore the combined effect of the stress changes and elastic rebounds on the accumulation of the horizontal displacement in the upper plate (Text S1) and earthquake triggering (Figure 4).

3.1 Time-variable surface displacements and slip over an analog earthquake and the early postseismic

Figure 1c and d visualizes the cumulative surface displacements averaged over the area above the seismogenic zone along the strike of the megathrust for both configurations (see Figures S2 & S3 for 2D surface displacement map). Figure 2a-b shows corresponding snapshots of the slip along the megathrust and upper plate fault (antithetic to the megathrust) inverted from surface displacements. The antithetic fault emerges in the upper plate in both configurations during the model evolution while rooted in the down-dip limit of the stick-slip patch(es). In the homogeneous system, the rupture initiates at one side of the stick-slip zone and laterally propagates as a pulse across it (Figures 1b and S2). While the rupture arrests on the opposite side, the early rupture area has apparently relocked and accumulates backslip at a higher rate than the plate convergence rate. This early backslip (slip reversal) on the megathrust reduces the cumulative trenchward surface displacement (Figure 1c). The lack of afterslip in the MSPs and the matrix immediately after the coseismic stage and the rearward surface displacement of the upper plate is evidence of a nearly complete stress-drop suggesting that the MSP is in its relocking phase.

In the heterogeneous system, the rupture nucleates in the matrix, where a small event first triggers the failure of the shallow patch followed by failure of the deeper patch (Figures 1d and S3). Because of the more localized ruptures limited to the MSPs, a sequence of two discontinuous crack-like failures is observed in contrast to the more continuous pulse-like event in the uniform model. Again, instantaneous relocking occurs in the shallow MSP while the deep MSP is still in the process of failing (Fig. 2a). The rearward displacement of the upper plate predominantly occurs at the site of the two moderate-size MSPs. In other words, the MSPs, which host large slips, undergo larger slip reversal than the matrix.

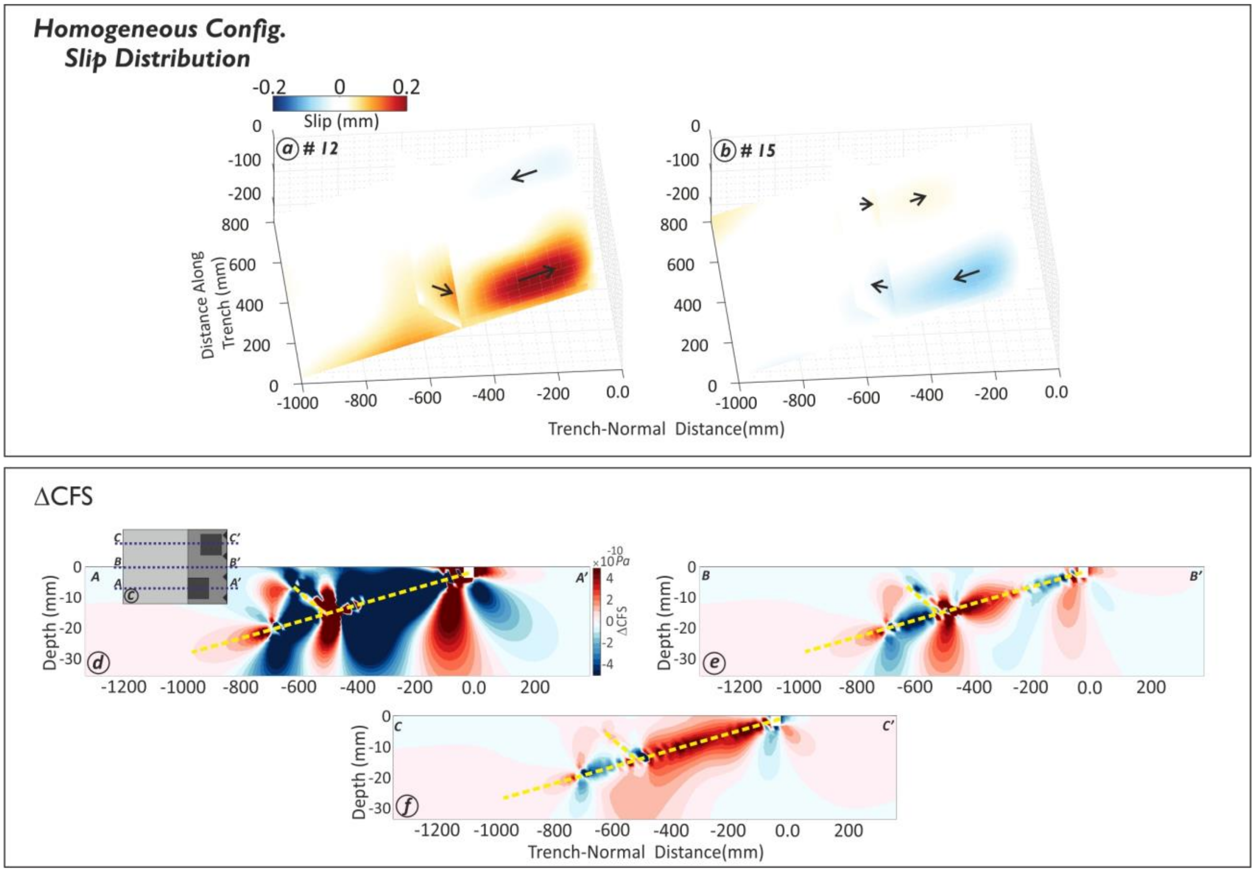

Figure 2. Upper panel: Slip models of the selected increments (marked in Figure 1d) in the heterogeneous system for demonstrating slip/backslip distribution in the MSPs and the antithetic upper plate fault. The vectors indicate the relative sense of slip but are not to scale. The lower panel represents three trench-normal profiles of Coulomb failure stress changes (ΔCFS) from the slip model snapshot #12 in the heterogeneous configuration. Inset shows the location of profiles on the model surface.

3.2 Coulomb failure stress changes

Based on the slip and backslip pattern documented above, we derive Coulomb failure stress changes (ΔCFS) (e.g., Lin and Stein, 2004) induced by the mainshock on the megathrust and the antithetic fault to get insight into zones of enhanced/decreased CFS (lower panel in Figure 2 and S4). We calculate the ΔCFS for the coseismic and postseismic stages of an event for the heterogeneous system on the receiver faults with the same sense and orientation as slip (Figure 2) and backslip (Figure S4) on the interface. In the shallow part of the plate interface (profile c-c'), a negative ΔCFS lobe is bounded by two positive ΔCFS lobes. The ΔCFS is highly enhanced at the upper limit of the rupture, where the shallow part of the interface ruptures and adjacent to the main slip zone on the slab. The ΔCFS on the normal faults (Figure S4) shows a decrease and an increase at the up-dip limit of the deep (in slip phase) and shallow (in backslip phase) MSPs on the slab, receptively. This early-postseismic enhancement may increase the tensional load in the slab (e.g., Lay *et al.*, 1989; Tilmann *et al.*, 2016) such that the postseismic extensional domain hosts the large normal mechanism aftershocks early after the megathrust event (e.g., Asano *et al.*, 2011; Lay *et al.*, 2011; Ruiz and Contreras-Reyes, 2015).

Another lobe of positive ΔCFS is extended to the down-dip limit of the main rupture area, where the antithetic fault in the upper plate appears during the model evolution (Figure 2). The deep-rooted antithetic fault, which imposes a significant discontinuity in the upper plate, perturbs the inner-wedge stress state and highly increases the CFS at the conjunction of the interface and the antithetic fault. Hence, it builds up stress and enhances the ΔCFS in the upper plate. However, the uncertainties in the slip distribution models at the conjugation zone may affect the ΔCFS's uncertainty. A relatively strong increase in CFS is predicted for the deeper MSP. Likely, it results from a combination of a backslip on the deeper MSP and the mainshock-induced stress transfer. However, the rapid backslip itself is the effect of the same induced stress transfer, as well.

3.3 Elastic rebound of upper plate and slab

We analyze the cumulative displacement fields of a few earthquake cycles for both configurations to reach an accurate view of the elastic responses from the slab and upper plate to the stress drop on the interface (Figure 3 and S5). In line with the *elastic rebound theory* (Reid, 1910), the coseismic strain release (i.e., shear-stress drop) leads to the rebound of the strained upper plate and slab, and transfers stress to the adjacent and nearby regions. The elastic response manifests itself in the kinetic energy consumed to accelerate both plates. The rebounds on the upper plate and slab (i.e., opposite sides of the megathrust interface) are in opposite directions (Savage, 1983). When we examine the velocity changes of the plates, we find that the model slab accelerates landward (Figures 3 & S5). The slab velocity increases by 50%-300% of the long-term velocity co- and early postseismically, depending on the event's magnitude. The magnitude of the events and slab accelerations indicate a positive correlation: the larger the earthquake is, the more significant is the response it generates (Figures 3 & S6). While we cannot measure the elastic rebound of the slab in the asperity area on the interface directly, these values should be considered minimum values of local slab acceleration.

3.4 Upper plate displacement accumulation

In both configurations, the postseismic backslip initiates immediately following the main event on the patches. The maximum amount of the backslip-caused surface displacement could reach 30% of the maximum coseismic surface displacement. The trench-normal surface displacements of the coseismic, postseismic, and interseismic stages of an earthquake cycle have been visualized in Figure S7. Comparing the magnitude of the cumulative surface velocities reveals that the horizontal surface displacement (mostly seafloor) during the early parts of the postseismic stage could reach up to 20-30% of the entire interseismic backslip.

In the upper plate, we observe a synthetic and kinematically consistent reactivation of the backthrust, i.e. as a normal fault during the coseismic megathrust slip phase and as a thrust in response to backslip on the megathrust. A slip ('trenchward') or back-slip rearward ('landward') on the interface may re-activate the antithetic fault in the upper plate with a normal (e.g., #12 in Figure 2a) and/or a reverse sense of movement (e.g., #15 in Figure 2b), respectively (Text S1). Following the slip distribution model (Figure 2a & b), two segments of the upper plate fault may move in opposite directions. This behavior likely reflects the shear sense on the MSPs. Particularly, in the upper plate fault, which in our experiments is rooted in the plate interface at the down-dip end of the seismogenic zone, the sense of slip (slip/backslip) on the seismogenic zone directly controls the slip mechanism of the antithetic fault. The coseismic and early postseismic upper-plate rotation (divergent mode versus convergent mode) has been discussed in Text S2.

4 Discussion and conclusion

4.1 Effect of the slab acceleration on the rapid relocking

Our simplified seismotectonic megathrust model suggests different rebounds (i.e., in terms of timing, magnitude, and direction) in the upper plate and slab triggering the immediate early-postseismic signals. An immediate relocking starts after rupture arrest and leads to a reversed surface displacement. While the rapid relocking is apparently limited on the two MSPs (in the heterogeneous system), it may postseismically reach a significant amount of the coseismic slip increments. The elastic response of the slab ("delayed rebound"), which comes into play as local acceleration, speeds up the stress build-up and results in this accelerated backslip. The large normal fault aftershocks in the slab following a megathrust event seaward of the megathrust event, such as occurring after the Maule (Ruiz & Contreras-Reyes, 2015) Tohoku-Oki earthquakes (Asano *et al.*, 2011; Lay *et al.*, 2011) reflect slab extension and thus the same elastic response of the slab. While the acceleration's impact appears as rearward surface displacements above the MSPs, the surface displacements above the matrix follow the slip sense of the MPSs in the heterogeneous configuration (Figures 2d and S3). The significant amount of the backslip suggests that the delayed rebound may not be the only possible mechanism involved in the rearward surface displacement. An extreme coseismic stress-drop overshoots the strained upper plate trenchward coseismically. The upper plate postseismically responds to this overshoot such that its elastic restoring force drags it back to a quasi-equilibrium state, which may appear as localized upper plate rearward surface displacements to a quasi-equilibrium state (Figure S8).

An immediate relocking and a high backslip velocity have been modeled based on land-limited GPS stations for the 2007 Pisco (Remy et al., 2016) and the 2010 Maule (Bedford et al., 2016) megathrust earthquakes, respectively. In the Tohoku-Oki earthquake region, the sparse sites directly above the high-slip zone postseimically moved landward faster than the pre-earthquake velocity (Tomita et al., 2015). This fast postseismic velocity has been explained via a slab acceleration driven by the recovery of force balance (Heki & Mitsui, 2013; Yuzariyadi & Heki, 2021) and the mantle relaxation (Sun et al., 2014; Watanabe et al., 2014). But it is expected that the mantle relaxation affects surface velocities at a relatively large wavelength. Also, the viscoelastic relaxation could not explain the trenchward motion of the stations above the slip zone further landward from the trench (Yuzariyadi & Heki, 2021). Afterslip might be the responsible mechanism for this surface displacement contrast at a relatively short distance (e.g., Sun & Wang, 2015; Tomita et al., 2017). Nevertheless, the coarse sampling rate of near-source observations prevents monitoring how the signals appear and evolve. Our analog model supports the occurrence of significant postseismic velocity changes with the slab deceleration following Omori-Utsu's decay law (Figure S5) of aftershock activity (Utsu et al., 1995). However, any viscoelastic behavior of the mantle may modify the elastic response of the slab and lead to a different response time scale. It means that the acceleration may last longer postseismically and decay with another characteristic time-constant in a coupled brittle-viscous system.

The stress evolution model for the extreme weakening observed during the Tohoku-Oki earthquake suggests a 20% slip reversal in the rupture's final stage, consistent with the postseismic stress stage derived from breakout data (Brodsky et al., 2020, 2017). However, our models suggest that the localized slip reversal may reflect the early postseismic stage due to a slab acceleration and/or a rapid restoration of the upper plate after experiencing elastic overshooting.

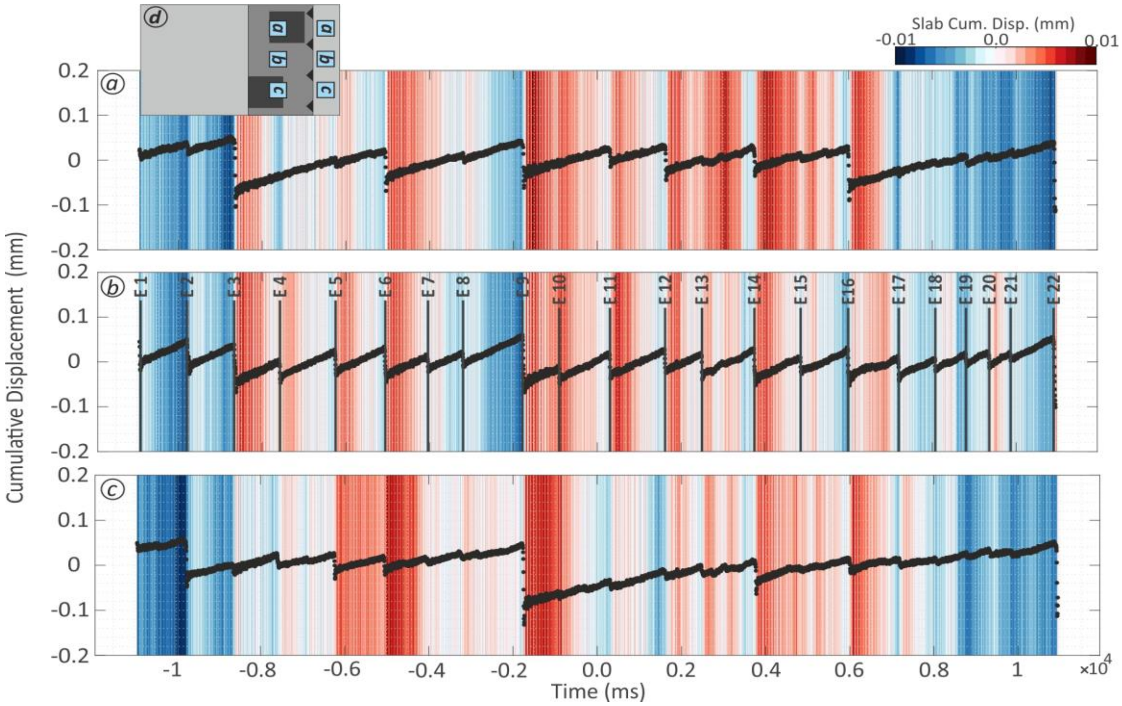

Figure 3. Upper plate time-series overlayed on the slab time-series (background colormap) from the heterogeneous configuration (see Figure S5 for the homogenous configuration). Note the location of the profiles relative to the upper plate and slab. The vertical lines (E1-E22) indicate abrupt surface displacement changes above the matrix. The warm color shows landward displacement of the slab. Larger events instigate greater slab responses (Figure S6).

4.2 Effects of the acceleration on event triggering

The stress enhancement on either receiver MSP (direct effect) or subducting plate (indirect effect) may bring the second MSP close to failure. In the heterogeneous configuration, the stress drop of the former event enhances ΔCFS on the second MSP, such that it directly increases the probability of failure. On the other hand, comparing the timing of slab acceleration and the latter event (T2 versus T3) shows that the acceleration occurs ahead of the later event. This interestingly suggests that the acceleration caused by the delayed elastic response of the slab has antedated the later event on the shallow MSP (Figures 4 & S9). Hence, the acceleration perturbs the MSP's seismic cycle and causes a “clock advance” in the loading cycle of the MSP (Figure S10).

The rupture of one asperity enhances the stress changes on the adjacent asperity and may bring it closer to failure. For example, Melnick *et al.* (2017) suggest that, besides static stress changes, the increased locking appears in segments adjacent to the failed asperity due to a combination of viscoelastic mantle relaxation and afterslip-controlled vertical axis rotation in the upper plate. The studies on the Wenchuan-Lushan sequential events on the Longmenshan fault show accelerated healing on an asperity in response to an earthquake on the adjacent asperity (Pei et al., 2019; Zhao et al., 2020). Accordingly, the enhanced postseismic compression and the accelerating accumulation of the elastic strain triggered the second event on the nearby asperity (Y. Li et al., 2018).

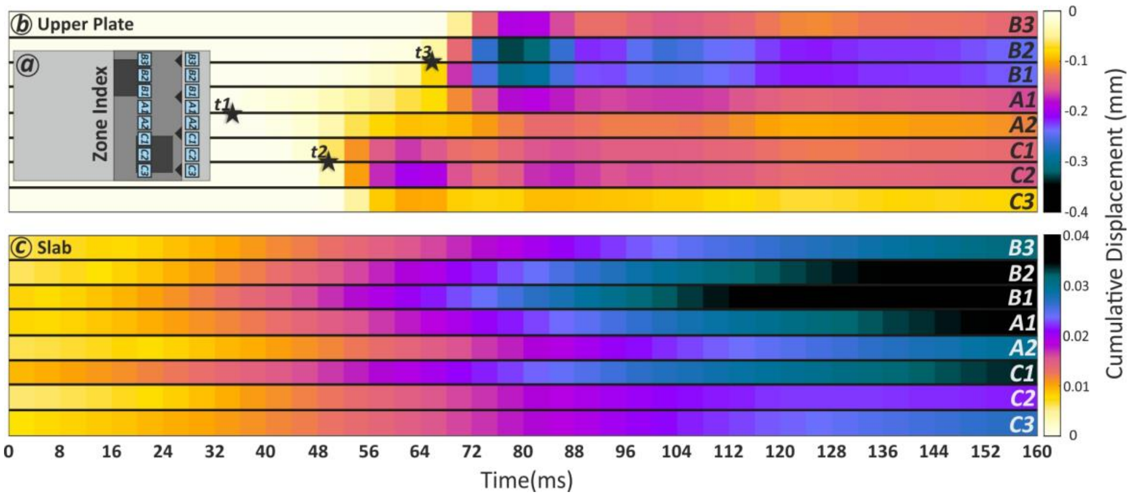

Figure 4. Timing of coseismic and postseismic elastic responses of the upper plate and slab for a representative event. a: relative location of the time-series on both plates shown as zone index; b: the elastic response of the upper-plate. t1 to t3 indicates the relative timing of the events; c: the elastic response of the slab.

Acknowledgment

All data in this study will be published open access soon (data archiving is underway). We thank GFZ Data Services for publishing the data. Meanwhile, the data set is uploaded as Supplemental Material 2 for review purposes. The research is supported by the SUBITOP Marie Sklodowska-Curie Action project from the European Union's EU Framework Programme for Research and Innovation Horizon 2020 (Grant Agreement 674899). The authors thank M. Rudolf and F. Neumann for their helpful discussion and assistance during our laboratory experiments.

References

Adam, J., Urai, J. L., Wieneke, B., Oncken, O., Pfeiffer, K., Kukowski, N., … Schmatz, J. (2005). Shear localisation and strain distribution during tectonic faulting—New insights from granular-flow experiments and high-resolution optical image correlation techniques. *Journal of Structural Geology*, *27*(2), 283–301.

Asano, Y., Saito, T., Ito, Y., Shiomi, K., Hirose, H., Matsumoto, T., … Sekiguchi, S. (2011). Spatial distribution and focal mechanisms of aftershocks of the 2011 off the Pacific coast of Tohoku Earthquake. *Earth, Planets and Space*, *63*(7), 669–673. https://doi.org/10.5047/eps.2011.06.016

Bedford, J., Moreno, M., Baez, J. C., Lange, D., Tilmann, F., Rosenau, M., … Vigny, C. (2013). A high-resolution, time-variable afterslip model for the 2010 Maule Mw = 8.8, Chile megathrust earthquake. *Earth and Planetary Science Letters*, *383*, 26–36. https://doi.org/10.1016/j.epsl.2013.09.020

Bedford, J., Moreno, M., Li, S., Oncken, O., Baez, J. C., Bevis, M., … Lange, D. (2016).

Separating rapid relocking, afterslip, and viscoelastic relaxation: An application of the postseismic straightening method to the Maule 2010 cGPS. *Journal of Geophysical Research: Solid Earth*, *121*(10), 7618–7638. https://doi.org/10.1002/2016JB013093

Bilek, S. L., & Lay, T. (2002). Tsunami earthquakes possibly widespread manifestations of frictional conditional stability. *Geophysical Research Letters*, *29*(14), 18–1. https://doi.org/10.1029/2002GL015215

Brodsky, E. E., Mori, J. J., Anderson, L., Chester, F. M., Conin, M., Dunham, E. M., … Yang, T. (2020). The State of Stress on the Fault Before, During, and After a Major Earthquake. *Annual Review of Earth and Planetary Sciences*, *48*(1), 49–74. https://doi.org/10.1146/annurev-earth-053018-060507

Brodsky, E. E., Saffer, D., Fulton, P., Chester, F., Conin, M., Huffman, K., … Wu, H.-Y. (2017). The postearthquake stress state on the Tohoku megathrust as constrained by reanalysis of the JFAST breakout data. *Geophysical Research Letters*, *44*(16), 8294–8302. https://doi.org/10.1002/2017GL074027

Caniven, Y., & Dominguez, S. (2021). Validation of a Multilayered Analog Model Integrating Crust-Mantle Visco-Elastic Coupling to Investigate Subduction Megathrust Earthquake Cycle. *Journal of Geophysical Research: Solid Earth*, *126*(2), e2020JB020342. https://doi.org/10.1029/2020JB020342

Chaves, E. J., Schwartz, S. Y., & Abercrombie, R. E. (2020). Repeating earthquakes record fault weakening and healing in areas of megathrust postseismic slip. *Science Advances*, *6*(32), eaaz9317. https://doi.org/10.1126/sciadv.aaz9317

Corbi, F., Sandri, L., Bedford, J., Funiciello, F., Brizzi, S., Rosenau, M., & Lallemand, S. (2019). Machine Learning Can Predict the Timing and Size of Analog Earthquakes. *Geophysical Research Letters*, *46*(3), 1303–1311. https://doi.org/10.1029/2018GL081251

Corbi, Fabio, Bedford, J., Sandri, L., Funiciello, F., Gualandi, A., & Rosenau, M. (2020). Predicting imminence of analog megathrust earthquakes with Machine Learning: Implications for monitoring subduction zones. *Geophysical Research Letters*, e2019GL086615.

Corbi, Fabio, Herrendörfer, R., Funiciello, F., & van Dinther, Y. (2017). Controls of seismogenic zone width and subduction velocity on interplate seismicity: Insights from analog and numerical models. *Geophysical Research Letters*, *44*(12), 6082–6091. https://doi.org/10.1002/2016GL072415

Heki, K., & Mitsui, Y. (2013). Accelerated pacific plate subduction following interplate thrust earthquakes at the Japan trench. *Earth and Planetary Science Letters*, *363*, 44–49. https://doi.org/10.1016/j.epsl.2012.12.031

Hicks, S. P., & Rietbrock, A. (2015). Seismic slip on an upper-plate normal fault during a large subduction megathrust rupture. *Nature Geoscience*, *8*(12), 955–960. https://doi.org/10.1038/ngeo2585

Hoffmann, F., Metzger, S., Moreno, M., Deng, Z., Sippl, C., Ortega-Culaciati, F., & Oncken, O. (2018). Characterizing Afterslip and Ground Displacement Rate Increase Following the 2014 Iquique-Pisagua Mw 8.1 Earthquake, Northern Chile. *Journal of Geophysical Research: Solid Earth*, *123*(5), 4171–4192. https://doi.org/10.1002/2017JB014970

Hoskins, M. C., Meltzer, A., Font, Y., Agurto-Detzel, H., Vaca, S., Rolandone, F., … Rietbrock, A. (2021). Triggered crustal earthquake swarm across subduction segment boundary after the 2016 Pedernales, Ecuador megathrust earthquake. *Earth and Planetary Science Letters*, *553*, 116620. https://doi.org/10.1016/j.epsl.2020.116620

Hsu, Y. J., Simons, M., Avouac, J. P., Galeteka, J., Sieh, K., Chlieh, M., … Bock, Y. (2006). Frictional afterslip following the 2005 Nias-Simeulue earthquake, Sumatra. *Science*, *312*(5782), 1921–1926. https://doi.org/10.1126/science.1126960

Kato, A., Sakai, S., & Obara, K. (2011). A normal-faulting seismic sequence triggered by the 2011 off the Pacific coast of Tohoku Earthquake: Wholesale stress regime changes in the upper plate. *Earth, Planets and Space*, *63*(7), 745–748. https://doi.org/10.5047/eps.2011.06.014

King Hubbert, M. (1937). Theory of scale models as applied to the study of geologic structures. *Bulletin of the Geological Society of America*, *48*(10), 1459–1520. https://doi.org/10.1130/GSAB-48-1459

Kosari, E., Rosenau, M., Bedford, J., Rudolf, M., & Oncken, O. (2020). On the Relationship Between Offshore Geodetic Coverage and Slip Model Uncertainty: Analog Megathrust Earthquake Case Studies. *Geophysical Research Letters*, *47*(15). https://doi.org/10.1029/2020GL088266

Lay, T., Ammon, C. J., Kanamori, H., Kim, M. J., & Xue, L. (2011). Outer trench-slope faulting and the 2011 Mw 9.0 off the Pacific coast of Tohoku Earthquake. *Earth, Planets and Space*, *63*(7), 713–718. https://doi.org/10.5047/eps.2011.05.006

Lay, T., Astiz, L., Kanamori, H., & Christensen, D. H. (1989). Temporal variation of large intraplate earthquakes in coupled subduction zones. *Physics of the Earth and Planetary Interiors*, *54*(3–4), 258–312. https://doi.org/10.1016/0031-9201(89)90247-1

Li, S., Moreno, M., Bedford, J., Rosenau, M., & Oncken, O. (2015). Revisiting viscoelastic effects on interseismic deformation and locking degree: A case study of the Peru-North Chile subduction zone. *Journal of Geophysical Research: Solid Earth*, *120*(6), 4522–4538. https://doi.org/10.1002/2015JB011903

Li, Y., Zhang, G., Shan, X., Liu, Y., Wu, Y., Liang, H., … Song, X. (2018). GPS-Derived Fault Coupling of the Longmenshan Fault Associated with the 2008 Mw Wenchuan 7.9 Earthquake and Its Tectonic Implications. *Remote Sensing*, *10*(5), 753. https://doi.org/10.3390/rs10050753

Lin, J., & Stein, R. S. (2004). Stress triggering in thrust and subduction earthquakes and stress interaction between the southern San Andreas and nearby thrust and strike-slip faults. *Journal of Geophysical Research: Solid Earth*, *109*(B2). https://doi.org/10.1029/2003jb002607

Loveless, J. P. (2017, February 16). Super-interseismic periods: Redefining earthquake recurrence. *Geophysical Research Letters*, Vol. 44, pp. 1329–1332. https://doi.org/10.1002/2017GL072525

Melnick, D., Moreno, M., Quinteros, J., Baez, J. C., Deng, Z., Li, S., & Oncken, O. (2017). The super-interseismic phase of the megathrust earthquake cycle in Chile. *Geophysical Research Letters*, *44*(2), 784–791. https://doi.org/10.1002/2016GL071845

Pei, S., Niu, F., Ben-Zion, Y., Sun, Q., Liu, Y., Xue, X., … Shao, Z. (2019). Seismic velocity reduction and accelerated recovery due to earthquakes on the Longmenshan fault. *Nature Geoscience*, *12*(5), 387–392.

Reid, H. F. (1910). The mechanism of the earthquake, the california earthquake of April 18, 1906, Report of the state earthquake investigation commission. In *Washington DC: Carnegie Institution* (Vol. 2).

Remy, D., Perfettini, H., Cotte, N., Avouac, J. P., Chlieh, M., Bondoux, F., … Socquet, A. (2016). Postseismic relocking of the subduction megathrust following the 2007 Pisco, Peru, earthquake. *Journal of Geophysical Research: Solid Earth*, *121*(5), 3978–3995. https://doi.org/10.1002/2015JB012417

Rosenau, M., Corbi, F., & Dominguez, S. (2017). *Analogue earthquakes and seismic cycles: experimental modelling across timescales. Solid Earth, European Geosciences Union*. *8*(3), 597–635. https://doi.org/10.5194/se-8-597-2017ï

Rosenau, M., Horenko, I., Corbi, F., Rudolf, M., Kornhuber, R., & Oncken, O. (2019). Synchronization of Great Subduction Megathrust Earthquakes: Insights From Scale Model Analysis. *Journal of Geophysical Research: Solid Earth*, *124*(4), 3646–3661. https://doi.org/10.1029/2018JB016597

Rosenau, M., Lohrmann, J., & Oncken, O. (2009). Shocks in a box: An analogue model of subduction earthquake cycles with application to seismotectonic forearc evolution. *Journal of Geophysical Research: Solid Earth*, *114*(1). https://doi.org/10.1029/2008JB005665

Rosenau, M., Nerlich, R., Brune, S., & Oncken, O. (2010). Experimental insights into the scaling and variability of local tsunamis triggered by giant subduction megathrust earthquakes. *Journal of Geophysical Research: Solid Earth*, *115*(9). https://doi.org/10.1029/2009JB007100

Rosenau, M., & Oncken, O. (2009). Fore-arc deformation controls frequency-size distribution of megathrust earthquakes in subduction zones. *Journal of Geophysical Research*, *114*(B10), B10311. https://doi.org/10.1029/2009JB006359

Ruiz, J. A., & Contreras-Reyes, E. (2015). Outer rise seismicity boosted by the Maule 2010 Mw 8.8 megathrust earthquake. *Tectonophysics*, *653*, 127–139. https://doi.org/10.1016/j.tecto.2015.04.007

Savage, J. C. (1983). A dislocation model of strain accumulation and release at a subduction zone. *Journal of Geophysical Research*, *88*(B6), 4984–4996. https://doi.org/10.1029/JB088iB06p04984

Sun, T., & Wang, K. (2015). Viscoelastic relaxation following subduction earthquakes and its effects on afterslip determination. *Journal of Geophysical Research: Solid Earth*, *120*(2), 1329–1344. https://doi.org/10.1002/2014JB011707

Sun, T., Wang, K., Iinuma, T., Hino, R., He, J., Fujimoto, H., … Hu, Y. (2014). Prevalence of viscoelastic relaxation after the 2011 Tohoku-oki earthquake. *Nature*, *514*(7520), 84–87. https://doi.org/10.1038/nature13778

Tilmann, F., Zhang, Y., Moreno, M., Saul, J., Eckelmann, F., Palo, M., … Dahm, T. (2016). The 2015 Illapel earthquake, central Chile: A type case for a characteristic earthquake? *Geophysical Research Letters*, *43*(2), 574–583. https://doi.org/10.1002/2015GL066963

Tomita, F., Kido, M., Ohta, Y., Iinuma, T., & Hino, R. (2017). Along-Trench variation in seafloor displacements after the 2011 Tohoku earthquake. *Science Advances*, *3*(7), e1700113. https://doi.org/10.1126/sciadv.1700113

Tomita, F., Kido, M., Osada, Y., Hino, R., Ohta, Y., & Iinuma, T. (2015). First measurement of the displacement rate of the Pacific Plate near the Japan Trench after the 2011 Tohoku-Oki earthquake using GPS/acoustic technique. *Geophysical Research Letters*, *42*(20), 8391–8397. https://doi.org/10.1002/2015GL065746

Uchida, N., & Bürgmann, R. (2019). Repeating earthquakes. *Annual Review of Earth and Planetary Sciences*, *47*, 305–332.

Utsu, T., Ogata, Y., S, R., & Matsu'ura. (1995). The Centenary of the Omori Formula for a Decay Law of Aftershock Activity. *Journal of Physics of the Earth*, *43*(1), 1–33. https://doi.org/10.4294/jpe1952.43.1

Wang, K., Hu, Y., & He, J. (2012). Deformation cycles of subduction earthquakes in a viscoelastic Earth. *Nature*, *484*(7394), 327–332. https://doi.org/10.1038/nature11032

Watanabe, S., Sato, M., Fujita, M., Ishikawa, T., Yokota, Y., Ujihara, N., & Asada, A. (2014). Evidence of viscoelastic deformation following the 2011 Tohoku-Oki earthquake revealed from seafloor geodetic observation. *Geophysical Research Letters*, *41*(16), 5789–5796. https://doi.org/10.1002/2014GL061134

Weiss, J. R., Qiu, Q., Barbot, S., Wright, T. J., Foster, J. H., Saunders, A., … Echalar, A. (2019). Illuminating subduction zone rheological properties in the wake of a giant earthquake. *Science Advances*, *5*(12), 6720–6738. https://doi.org/10.1126/sciadv.aax6720

Yuzariyadi, M., & Heki, K. (2021). Enhancement of interplate coupling in adjacent segments after recent megathrust earthquakes. *Tectonophysics*, *801*, 228719. https://doi.org/10.1016/j.tecto.2021.228719

Zhao, J., Ren, J., Liu, J., Jiang, Z., Liu, X., Liang, H., … Yuan, Z. (2020). Coupling fraction and relocking process of the Longmenshan Fault Zone following the 2008 Mw7. 9 Wenchuan earthquake. *Journal of Geodynamics*, 101730.